Article

Effect of Post Heat Treatment on the Microstructure and Microhardness of Friction Stir Processed NiAl Bronze (NAB) Alloy

Yuting Lv, Liqiang Wang *, Xiaoyan Xu and Weijie Lu *

State Key Laboratory of Metal Matrix Composites, Shanghai Jiao Tong University, Shanghai 200240, China; E-Mails: lyt8608@sjtu.edu.cn (Y.L.); xuxiaoyan727@sjtu.edu.cn (X.X.)

* Authors to whom correspondence should be addressed;
   E-Mails: wang_liqiang@sjtu.edu.cn (L.W.); luweijie@sjtu.edu.cn (W.L.);
   Tel.: +86-21-3420-2641 (L.W.); Fax: +86-21-3420-2749 (L.W.).

Academic Editor: Anders E. W. Jarfors

Abstract: NiAl bronze (NAB) alloy is prepared by using friction stir processing (FSP) technique at a tool rotation rate of 1200 rpm and a traverse speed of 150 mm/min. A post heat treatment is performed at the temperature of 675 °C. The effect of heat treatment on the microstructure and microhardness is studied. The results show that the microstructure of the FSP NAB alloy consists of high density dislocations, retained β phase (β′ phase) and recrystallized grains. When annealed at 675 °C, discontinuous static recrystallization (DSRX) takes place. The content of β′ phase gradually decreases and fine κ phase is precipitated. After annealing for 2 h, both the microhardness of the FSP sample in the stir zone (SZ) and the difference in hardness between the SZ and base metal decrease due to the reduction of the dislocation density and β′ phase, accompanying recrystallized grain coarsening. With further increasing of the annealing time to 4 h, the aforementioned difference in hardness nearly disappears.

Keywords: NiAl bronze (NAB); friction stir processing (FSP); heat treatment; micro-hardness

1. Introduction

Nickel-aluminum bronze (NAB) alloy is one kind of copper-aluminum alloys. Due to high strength and excellent corrosion resistance, this alloy is widely used for marine equipment such as propellers, pumps, valves, *etc.* [1]. Under normal casting conditions, the microstructure is composed of α phase, several intermetallic phases (κI, κII, κIII, and κIV) and a retained β phase (β′ phase) [2]. Nakhaie *et al.* [3] found that the anodic character of κ phase with tens of millivolt is higher than that of copper-rich α phase, which increases the galvanic corrosion resistance of NAB alloy. In addition, the NAB alloy is reported to be susceptible to crevice and selective phase corrosion [4].

Recently, several techniques have been used to improve both the corrosion resistance and mechanical properties of cast NAB alloy, such as equal channel angular extrusion (ECAE) [5,6], laser surface melting (LSM) [7,8], and friction surfacing (FS) [9]. Tang *et al.* [8] reported that laser surface melting improved the corrosion resistance and erosion resistance of cast manganese-nickel-aluminum bronze due to the formation of a homogeneous and single phase microstructure. Hanke *et al.* [9] found that FS could improve the cavitation erosion of NAB because fine grains and homogeneous microstructure are obtained during friction surfacing.

Friction stir processing (FSP) is a solid state metal working technique which was developed based on the basic principle of friction stir welding (FSW) [10]. During the FSP process, the specimen undergoes intense plastic deformation at simultaneously-elevated temperature, resulting in the formation of fine and equiaxed recrystallized grains. This method has been widely used to localize microstructure modification in wrought, powder metallurgy and cast materials due to its energy efficiency, being environmentally-friendly, and versatility [11]. Microstructural evolution and mechanical properties of FSP NAB alloy have been studied in many literatures. Swaminathan *et al.* [12] found that the peak temperature in the stir zone during FSP was 92% to 97% of the melting point. At "low" temperature, NAB undergoes intense plastic deformation during FSP, leading to grain refinement and microstructure uniformity. According to the previous literature, the refined grains and homogeneous microstructure can improve the mechanical properties of the NAB alloy [13,14]. The corrosion resistance of FSP NAB alloy is also enhanced by the refined grains [15]. Song *et al.* [16] found that FSP NAB suffers less severe attack than the as-cast NAB because FSP reduces the Volta potential difference among all the constituent phases in as-cast NAB. Moreover, the retained β phase can be produced when cooled at a high cooling rate, which has a harmful effect on the corrosion properties due to its direct contact with the cathodic sites and its martensitic structure [16]. Lenard *et al.* [17] also reported that the NAB composed of more β′ phase could produce pit corrosion after long-time exposure to sea water. In the previous literature, β′ phase can be restrained by means of heat treatment [18]. However, post heat treatment of FSP NAB alloy has yet rarely been studied.

In this study, as-cast NAB alloy is produced by FSP and post heat treated at 675 °C for 2 or 4 h, and the effect of post heat treatment on the microstructure and microhardness of FSP NAB alloy is studied.

2. Experimental Procedure

As-cast Cu-9.5Al-4.2Ni-4Fe-1.2Mn NAB alloy ingot with a dimension of ϕ 150 mm × 100 mm was prepared by non-vacuum melting and is then forged to a block sample with the cross section dimension

of 150 mm × 30 mm at 850 °C. The microstructure of the forged specimen consists of α, κ$_{II}$, κ$_{IV}$, and retained β phases, as shown in Figure 1. The FSP was carried out at a tool rotation rate (ω) of 1200 rpm and traverse speed (υ) of 150 mm/min with continuously flowing argon gas around the rotating tool to prevent surface oxidation. A tungsten carbide-based alloy tool was used, which had a 15 mm-diameter concaved shoulder, 7 mm-diameter unthreaded pin, a 2 mm pin height, and tilted by 2.5°. The FSP samples were heated up to 675 °C for 2 and 4 h, respectively, then air cooled. The samples were cut, cold mounted, grounded, polished, and then etched by a solution of 5 g FeCl$_3$ + 2 mL HCl + 95 mL C$_2$H$_5$OH. Microstructural features of as-FSP and post-FSP heat treated samples were observed using optical microscopy (OM, Leica MEF4M, Wetzlar, Germany) and JEOL 7600-F field emission gun scanning electron microscope (SEM, JEM-2100F, Tokyo, Japan). Phase constituents were identified by a D8 ADVANCE X-ray diffractometer (XRD, D/max-IIIA, Tokyo, Japan) with Cu K$_α$ radiation at room temperature. Vickers microhardness was measured on the polished cross-section using an automated tester with a load of 500 g. A JEM-200 EX transmission electron microscope (TEM, JEM-2100F, Tokyo, Japan) was used to characterize the microstructure of heat treated FSP NAB samples. For TEM sample preparation, thin plates were cut from the samples and then mechanically polished to 100 μm. The polished thin plates were finally twin-jet electro-polished to make electron beam transparent thin films, using a solution of 33% nitric acid and 67% methanol (in volume fraction) at −25 °C.
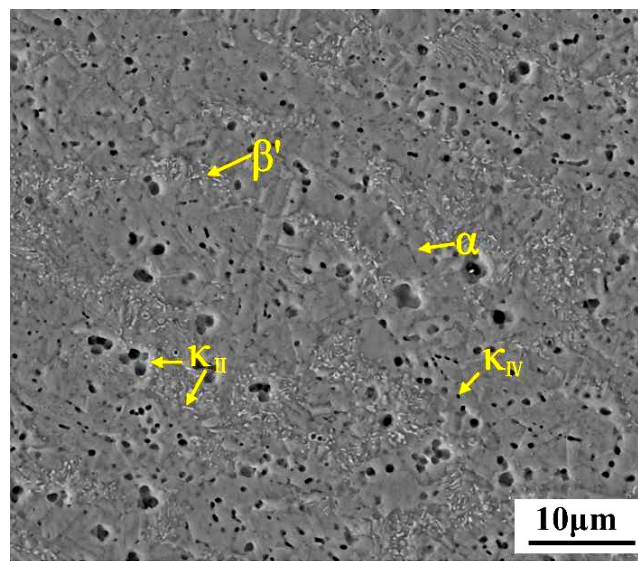

Figure 1. Initial microstructure of forged NAB alloy.

3. Results and Discussion

Figure 2 shows the microstructure of the FSP NAB alloy obtained at a rotation rate of 1200 rpm and traverse speed of 150 mm/min. As can be seen from Figure 2a, the microstructure in SZ is inhomogeneous, as indicated by region A, B, and C respectively. The enlarged inhomogeneous microstructure is shown in Figure 2b,c, and d respectively. The depth of region A is about 1 mm and the microstructure contains Widmanstatten α and β′ phases (Figure 2b). The fine κ$_{II}$ phase is also found in the enlarged image of this region (Figure 3a). In region B and C, the microstructure also contains α, fine κ$_{II}$, and β′ phases, while the α phase has different morphologies between regions B and C. The morphology of α phase in region B is banded and that in region C is stream-like. According to

Ni's study [19,20], the banded and stream-like α structure results from the incomplete dynamic recrystallization and intense plastic deformation during friction stir processing.
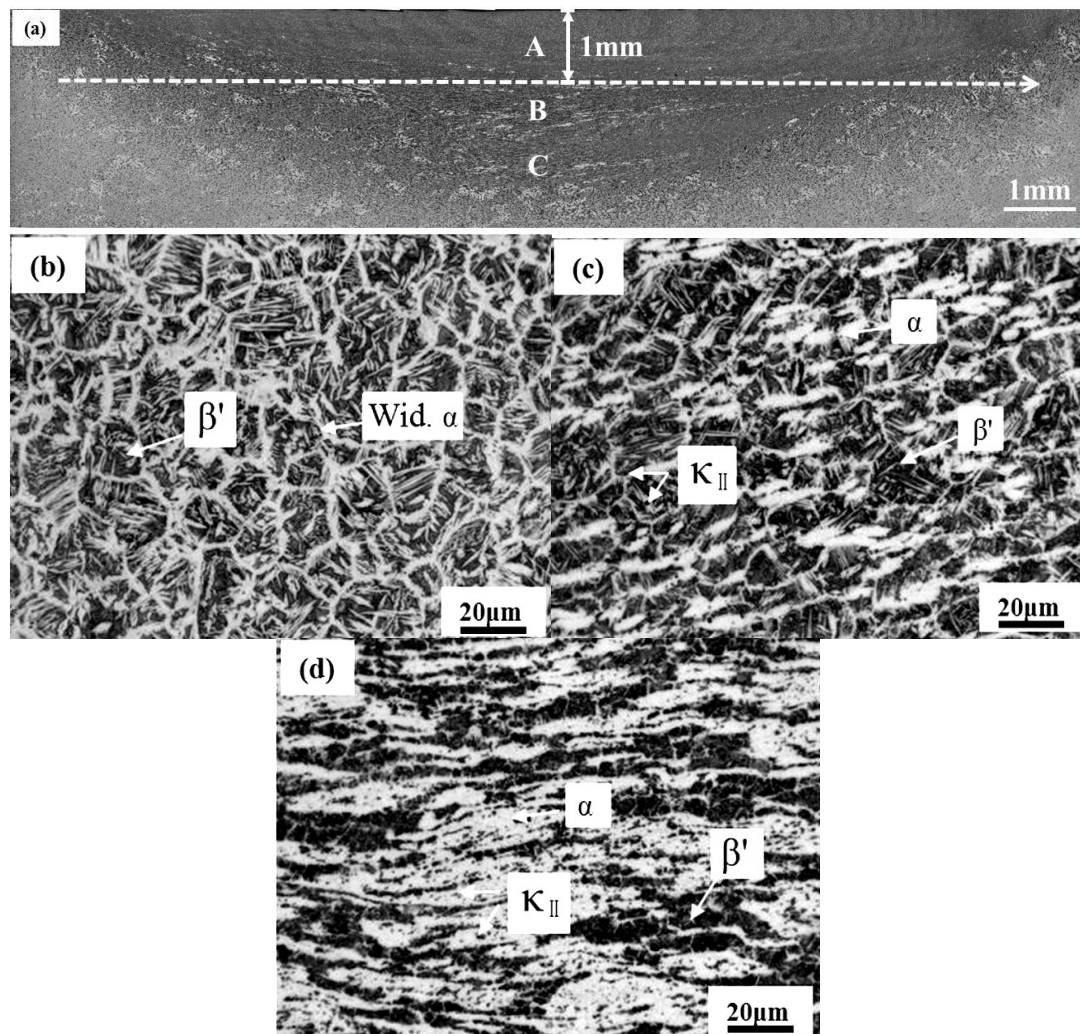

Figure 2. OM images showing the microstructure of FSP NAB alloy. (**a**) Profile. (**b**) Region A in Figure 2a. (**c**) Region B in Figure 2a. (**d**) Region C in Figure 2a.

Figure 3 shows the microstructures of the FSP NAB and post heat treated samples. In Figure 3b, α grains boundaries and fine voids are clearly observed. The morphologies of voids can be classified into three types; they are globular shape, lamellar shape in α grains, triangular shape in grain boundaries, or triple points of grains. The globular or lamellar shape void is the κ phase that is precipitated during the annealing process and the triangular shape void is the remaining β′ phase due to less annealing time, which indicates that most β′ phase transforms to α and fine κ phases when the FSP NAB is annealed at 675 °C for 2 h. Figure 3c shows the microstructure of the FSP NAB annealed for 4 h. As can be seen, the β′ phase disappears and more κ phases appear, which also reveals that β′ phase fully transforms to α and fine κ phases.
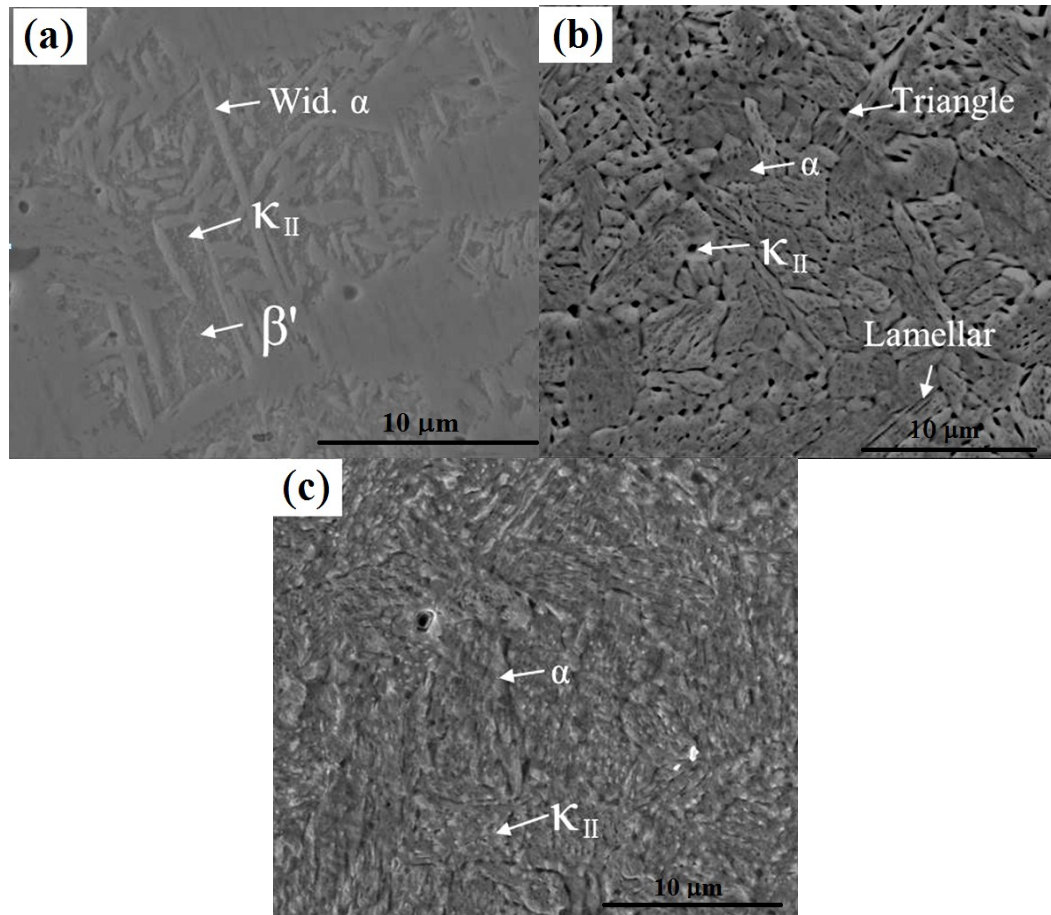
Figure 3. The microstructures of FSP NAB and post heat treated conditions (Region A in Figure 2). (**a**) FSPed NAB alloy. (**b**) Annealing 2 h. (**c**) Annealing 4 h.

Figure 4 shows the XRD patterns of FSP NAB and heat treated samples. As can be seen, the XRD profile of the FSP NAB has lower α (Cu) and (Fe, Ni) Al peaks, which increase significantly after annealing for 2 h. With further increasing of the annealing time to 4 h, a similar XRD profile is obtained. This indicates that most β′ phase transforms to α and/or κ phases when the FSP NAB alloy is annealed for 2 h. With further increasing of the annealing time, a small amount of β′ phase transforms to α and/or κ phases, which has little influence on the XRD pattern. This result is consistent with the former microstructure observations in Figure 3.
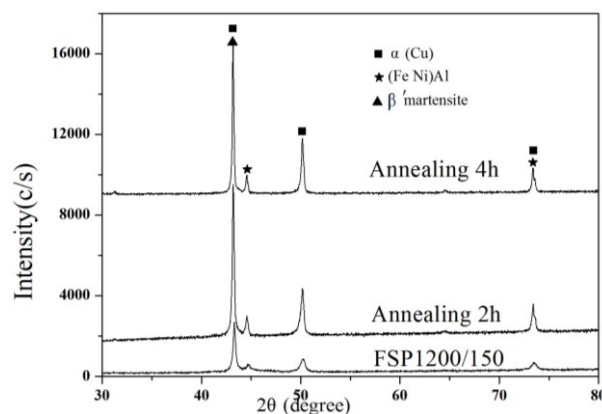

Figure 4. The X-ray diffraction patterns of FSP NAB and post heat treated conditions.

Microhardness tests on the FSP NAB and post heat treated samples are performed along the arrow direction (see Figure 2a). As observed in Figure 5, the SZ of FSP NAB exhibits extremely high microhardness of about 290 HV, which is much higher than that in matrix. This indicates that FSP significantly promotes the microhardness of NAB alloy. After annealing for 2 h, the microhardness of SZ obviously decreases, which is about 235 HV. With further increasing of the annealing time to 4 h, the microhardness of SZ decreases slightly which suggests that the microhardness reaches a steady state. It is worth mentioning that the difference in microhardness between SZ and matrix decrease with the increase in annealing time and such a difference almost diminishes when increasing the annealing time to 4 h.
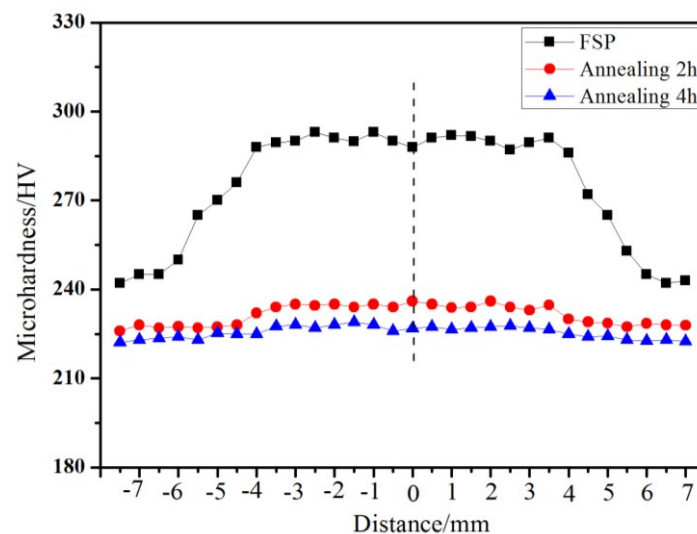

Figure 5. Microhardness variations as a function of distance from center line for FSP NAB alloy and post heat treated conditions.

In order to understand the variation in microhardness with the increase in annealing time, TEM observations of FSP NAB and post heat treated samples are carried out. Figure 6a shows the TEM images of the FSP NAB, in which the recrystallized grains are well-distributed in high density dislocations. This indicates that there are large quantities of dislocations although recrystallization occurs at the region of high store energy. The high density dislocations may be the main reason responsible for the higher microhardness of FSP NAB alloy. Figure 6b,c show the TEM images of the FSP NAB annealed for 2 h and 4 h. Compared with FSP NAB, the amount of recrystallized grains increases and the quantity of work-hardening regions decreases (Figure 6b), which clearly shows that discontinuous static recrystallization (DSRX) occurs during post heat treatment [21]. With further increasing of the annealing time to 4 h, coarse grains and few dislocations are observed (See Figure 6c). It is suggested that the effect of work hardening decreases with the increase in the annealing time, and disappears when FSP NAB is annealed for 4 h, which can also explain the gradual decrease of microhardness.

Figure 6d shows the microstructure of β′ phase obtained during FSP. As can be seen, the β′ phase is presented as twin morphology, which may contribute to strengthen the FSP NAB by acting as a grain boundary, blocking lattice dislocation motion [22]. A large quantity of β′ phase is observed in the FSP NAB alloy, which may be another reason for the higher microhardness. After annealing for 2 h,

dislocation-free and high-density dislocation regions are clearly observed (see Figure 6e). This indicates that dislocation motion occurs and the amount of β′ phase decreases during annealing. Figure 6f shows the TEM images of the FSP NAB heat treated for 4 h, in which the fine κ phase is distributed in coarser α grains. This reveals that, with further increasing the annealing time, recrystallized grains grow gradually and the fine κ phase is precipitated in the α grains. This result is consistent with the SEM observations (see Figure 4c). The gradual decrease in content of β′ phase is also responsible for the decrease in microhardness.
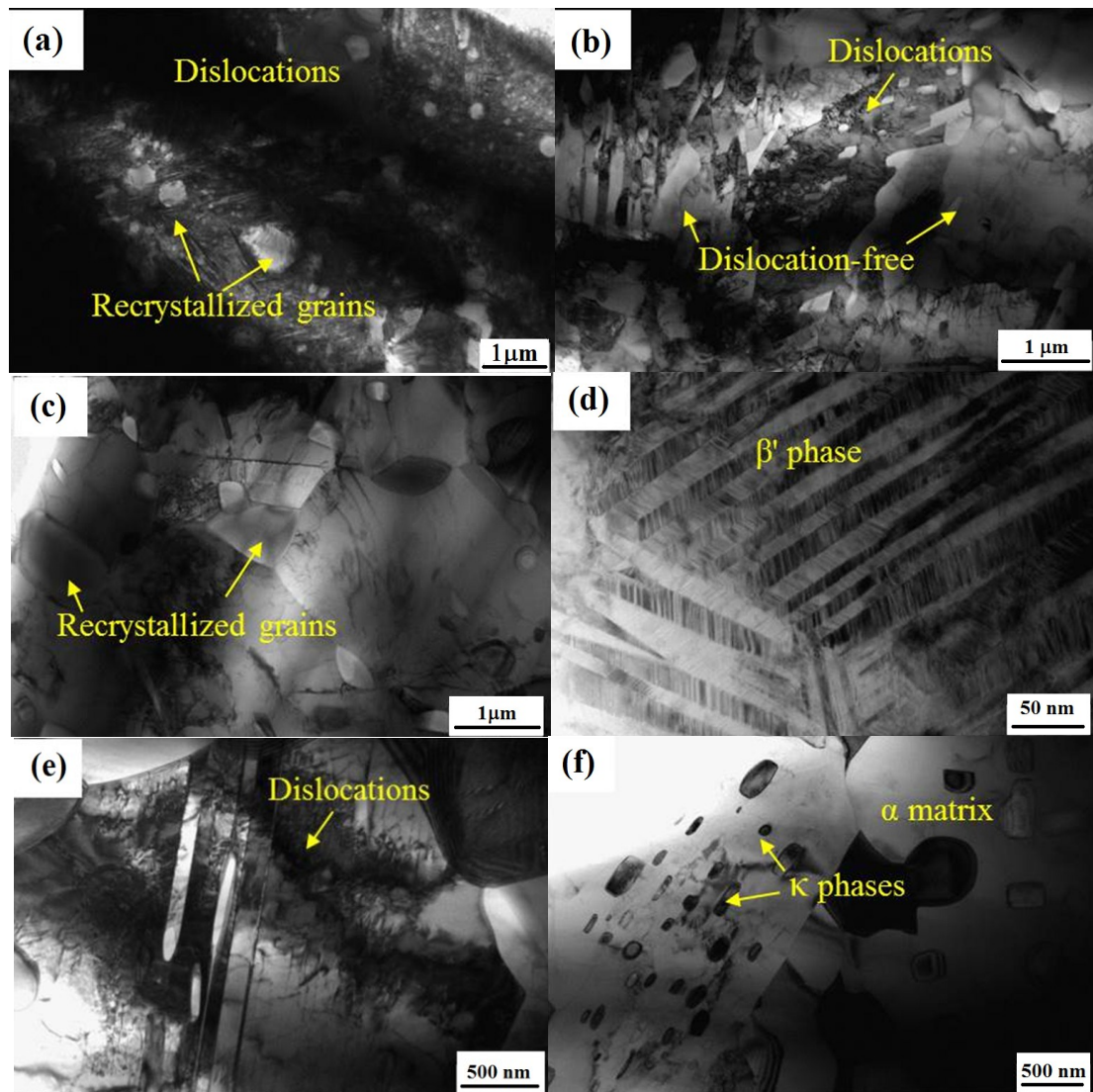

Figure 6. TEM images of (**a**) and (**d**) FSP NAB and post heat treated by annealing for: (**b**) and (**e**) 2 h, and (**c**) and (**f**) 4 h.

4. Conclusions

In this study, as-cast NAB alloy is produced by FSP, and is then heat treated at 675 °C for 2 and 4 h, respectively. The effect of post heat treatment on the microstructure and microhardness of FSP NAB alloy is studied. The microstructure of the FSP NAB alloy contains high-density dislocations, β′ phase, and recrystallized grains. During annealing, discontinuous static recrystallization occurs. The β′ phase disappears gradually, the fine κ phase is precipitated with the increase in annealing time, and the

microhardness of FSP NAB alloy decreases. The gradual decrease in microhardness is mainly attributed to the decrease in dislocation density and β′ phase accompanying recrystallized grain coarsening. The difference in microhardness between SZ and matrix decreases with the increase in annealing time, which will diminish as the annealing time increases to 4 h. The β′ phase of the FSP NAB alloy can be reduced by heat treatment, which will have a favorable effect on the improvement of the corrosion resistance of the FSP NAB alloy.

Acknowledgments

Author Contributions

Yuting Lv performed the experiments and wrote the paper under Liqiang Wang and Weijie Lu's guidance, and contributed to all activities; Xiaoyan Xu contributed to the interpretation and discussion of results.

Conflicts of Interest

The authors declare no conflict of interest.

References

1. Hasan, F.; Jahanafrooz, A.; Lorimer, G.W.; Ridley, N. The morphology, crystallography and chemistry of phases in as cast nickel aluminum bronze. *Metall. Mater. Trans. A* **1982**, *13*, 1337–1345.
2. Jahanafrooz, A.; Hasan, F.; Lorrmer, G.W.; Ridley, N. Microstructural development in complex nickel aluminum bronzes. *Metall. Mater. Trans. A* **1982**, *14*, 1951–1956.
3. Nakhaie, D.; Davoodi, A.; Imani, A. The role of constituent phases on corrosion initiation of NiAl bronze in acidic media studied by SEM–EDS, AFM and SKPFM. *Corros. Sci.* **2014**, *80*, 104–110.
4. Wharton, J.A.; Stokes, K.R. The influence of nickel–aluminium bronze microstructure and crevice solution on the initiation of crevice corrosion. *Electrochim. Acta* **2008**, *53*, 2463–2473.
5. Gao, L.L.; Cheng, X.H. Microstructure and dry sliding wear behavior of Cu–10%Al–4%Fe alloy produced by equal channel angular extrusion. *Wear* **2008**, *265*, 986–991.
6. Gao, L.L.; Cheng, X.H. Microstructure and mechanical properties of Cu–10%Al–4%Fe alloy produced by equal channel angular extrusion. *Mater. Des.* **2008**, *29*, 904–908.
7. Tang, C.H.; Cheng, F.T.; Man, H.C. Effect of laser surface melting on the corrosion and cavitation erosion behaviors of a manganese–nickel–aluminium bronze. *Mater. Sci. Eng. A* **2004**, *373*, 195–203.
8. Tang, C.H.; Cheng, F.T.; Man, H.C. Improvement in cavitation erosion resistance of a copper-based propeller alloy by laser surface melting. *Surf. Coat. Technol.* **2004**, *182*, 300–307.

9. Hanke, S.; Fischer, A.; Beyer, M.; Santos, J.D. Cavitation erosion of NiAl-bronze layers generated by friction surfacing. *Wear* **2011**, *273*, 32–37.

10. Mishra, R.S.; Ma, Z.Y. Friction stir welding and processing. *Mater. Sci. Eng. R* **2005**, *50*, 1–78.

11. Nandan, R.; Debroy, T.; Bhadeshia, H. Recent advances in friction stir welding process, weldment structure and properties. *Prog. Mater. Sci.* **2008**, *53*, 980–1023.

12. Swaminathan, S.; Oh-Ishi, K.; Zhilyaev, A.P.; Fuller, C.B.; London, B.; Mahoney, M.W.; Mcnelley, T.R. Peak Stir Zone Temperatures during Friction Stir Processing. *Metall. Mater. Trans. A* **2009**, *41*, 631–640.

13. Oh-ishi, K.; Mcnelley, T.R. Microstructural modification of as-cast Ni Al bronze stir processing. *Metall. Mater. Trans. A* **2004**, *35*, 2951–2960.

14. Su, J.; Swaminthan, S.; Menon, S.K.; Mcnelley, T.R. The effect of concurrent straining on phase transformations in NiAl bronze during the friction stir processing thermomechanical Cycle. *Metall. Mater. Trans. A* **2011**, *42*, 2420–2430.

15. Ni, D.R.; Xiao, B.L.; Ma, Z.Y.; Qiao, Y.X.; Zheng, Y.G. Corrosion properties of friction stir processed cast NiAl bronze. *Corros. Sci.* **2010**, *52*, 1610–1617.

16. Song, Q.N.; Zheng, Y.G.; Ni, D.R.; Ma, Z.Y. Studies of the nobility of phases using scanning Kelvin probe microscopy and its relationship to corrosion behaviour of Ni–Al bronze in chloride media. *Corro. Sci.* **2014**, *92*, 95–103.

17. Lenard, D.R.; Bayley, C.J. Electrochemical monitoring of selective phase corrosion of NiAl bronze in Seawater. *Corrosion* **2008**, *64*, 764–772.

18. Anantapong, J.; Uthaisangsuk, V.; Suranuntchai, S.; Manonukul, A. Effect of hot working on microstructure evolution of as-cast Nickel Aluminum Bronze alloy. *Mater. Des.* **2014**, *60*, 233–243.

19. Ni, D.R.; Xue, P.; Wang, D.; Xiao, B.L.; Ma, Z.Y. Inhomogeneous microstructure and mechanical properties of friction stir processed NiAl bronze. *Mater. Sci. Eng. A* **2009**, *524*, 119–128.

20. Ni, D.R.; Xue, P.; Ma, Z.Y. Effect of Multiple-Pass Friction Stir Processing Overlapping on Microstructure and Mechanical Properties of As-Cast NiAl Bronze. *Metall. Mater. Trans. A* **2011**, *42*, 2125–2135.

21. Sakai, T.; Belyakov, A.; Kaibyshev, R.; Miura, H.; Jonas, J.J. Dynamic and post-dynamic recrystallization under hot, cold and severe plastic deformation conditions. *Prog. Mater. Sci.* **2014**, *60*, 130–207.

22. Lu, K.; Lu, L.; Suresh, S. Strengthening materials by engineering coherent internal boundaries at the nanoscale. *Science* **2009**, *324*, 349–352.